Chin. Geogra. Sci. 2021 Vol. 31 No. 5 pp. 915−930
https://doi.org/10.1007/s11769-021-1233-5

Springer Science Press
www.springerlink.com/content/1002-0063

Aspect in Topography to Enhance Fine-detailed Landform Element Extraction on High-resolution DEM

XIE Xiao[1, 2, 3, 4], ZHOU Xiran[1, 3], XUE Bing[2], XUE Yong[1, 3], QIN Kai[1, 3], LI Jingzhong[2], YANG Jun[5]

(1. *School of Environment Science and Spatial Informatics*, *China University of Mining and Technology*, *Xuzhou* 221116, *China*; 2. *Key Lab for Environmental Computation and Sustainability of Liaoning Province*, *Institute of Applied Ecology*, *Chinese Academy of Sciences*, *Shenyang* 110016, *China*; 3. *Artificial Intelligence Research Institute*, *China University of Mining and Technology*, *Xuzhou* 221116, *China*; 4. *School of Geodesy and Geomatics*, *Wuhan University*, *Wuhan* 430072, *China*; 5. *JangHo Architecture*, *Northeastern University*, *Shenyang* 110169, *China*)

Abstract: The value of the high-resolution data lies in the high-precision information discovery. The fine-detailed landform element extraction is thus the basis of high-fidelity application of the high-resolution digital elevation models (DEMs). However, the results of landform element extraction generated by classical methods might be ungrounded on high-resolution DEMs. This paper presents our research on using the aspect to reinforce the applicability and robustness of the classical approaches in landform element extraction. First, according to the research of pattern recognition, we assume that aspect-enhanced landform representation is robust to rotation, scaling and affine variance. To testify the role of aspect, we respectively integrated the aspect into three classical approaches: mean curvature-based fuzzy classification, elevation-based feature descriptor, and object-based segmentation. In the experiment, based on four types of high-resolution DEMs (1 m, 2 m, 4 m and 8 m), we compare each classical approaches and their corresponding aspect-enhanced approaches based on extracting the rims of two craters having different landforms, and the ridgelines and valleylines of a region covered by few vegetables and man-made buildings. In comparison to the results generated by curvature-based fuzzy classification, the aspect enhanced curvature-based fuzzy classification can effectively filter a number of noises outperforms the curvature-based one. Otherwise, the aspect-enhanced feature descriptor can detect more landform elements than the elevation-based feature descriptor. Moreover, the aspect-based segmentation can detect the main structure of landform, while the boundaries segmented by classical approaches are messing and meaningless. The systematic experiments on meter-level resolution DEMs proved that the aspect in topography could effectively to improve the classical method-system, including fuzzy-based classification, feature descriptors-based detection and object-based segmentation. The value of aspect is significantly great to be worthy of attentions in landform representation.

Keywords: high-resolution DEM (digital elevation model); landform representation; landform element extraction; crater detection; aspect granularity; aspect-enhanced landform representation; America

Citation: XIE Xiao, ZHOU Xiran, XUE Bing, XUE Yong, QIN Kai, LI Jingzhong, YANG Jun, 2021. Aspect in Topography to Enhance Fine-detailed Landform Element Extraction on High-resolution DEM. *Chinese Geographical Science*, 31(5): 915−930. https://doi.org/10.1007/s11769-021-1233-5

1 Introduction

Digital elevation model (DEM) is an important data product to characterize the three-dimensional representation of landforms. Currently, massive multi-resolution DEMs were made available for public use thanks for the

Received date: 2020-12-18; accepted date: 2021-04-08
Foundation item: Under the auspices of Priority Academic Program Development of Jiangsu Higher Education Institutions (No. 140119001), Science & Technology Department of Liaoning Province (No. 20180550831)
Corresponding author: ZHOU Xiran. E-mail: xrzhou@cumt.edu.cn

progress of earth observation techniques (Liu, 2008; Deilami and Hashim, 2011; Rossi et al., 2012; Tao et al., 2012; Tarolli and Sofia, 2016; Arundel et al., 2018; Yang et al., 2019). Since the boundaries of landform are impossible to be accurately determined (Evans, 2012), many criteria and classification systems regarding landform element have been proposed by measuring the distance in surface and elevation from DEM, such as classification of form elements (Dikau, 1989), morphometric features classes (Wood, 1996), rule base of 15 unit landform classification (MacMillan et al., 2000), classification of 15 landform elements based on local slope and curvature (Schmidt and Hewitt, 2004), landform classes based on multiple types of curvature (MacMillan and Shary, 2009), Shary's complete system of classification, morphometric features classification based on slope categories (Ehsani and Quiel, 2008), 10 most common landform elements (Jasiewicz and Stepinski, 2013). Landform element has become the critical units for landform characterization.

Currently, high resolutions DEMs, especially very-high resolution DEMs, provide great support for fine-detailed landforms element extraction, which would be critical for recording land surface. In order to automatically and quickly extract landform elements, elevation and its derivatives including curvature, slope, hillshade, aspect, *etc*. have been used as the parameters (Drăguţ and Eisank, 2011; Jasiewicz and Stepinski, 2013; Zhu et al., 2014; 2019; Qian et al, 2016). The techniques proposed by these works include edge detection, fuzzy classification (Drăguţ and Blaschke, 2006; van Asselen and Seijmonsbergen, 2006), object-based segmentation (Drăguţ and Blaschke, 2006; Drăguţ and Eisank, 2011; Romstad and Etzelmüller, 2012), hydrological analysis (Chaplot et al., 2006; Murphy et al., 2008), feature descriptor (Jasiewicz and Stepinski, 2013), and applied data of elevation, curvature and/or slope.

However, the complicated and fine-detailed land surfaces are represented significantly different between moderate or low-resolution and high-resolution DEMs. There includes 'less noise' and the land surface is much smoother in such data (Tarolli, 2014; Liu et al., 2017; Szypuła, 2019). Although the existing methods regarding landform element extraction, such as fuzzy classification, feature descriptor and object segmentation, are suitable for medium- or low-resolution DEMs, they might perform weakly in noisy background when the surface details are obtained from high-resolution DEMs. For example, when the details of land surface are available from high-resolution DEMs (i.e., rocks, trees, small-scale hillsides and creeks), artificial substances and other irrelevant terrain objects might be seen on two sides of a ridge or a valley, making both ridgeline/valleyline and all these irrelevant features be extracted.

Although curvature is an important derivative of elevation widely being used for landform element extraction (Schmidt and Andrew, 2005; Pirotti and Tarolli, 2010; Romstad and Etzelmüller, 2012), it might not be proficient in high-resolution DEMs (Zhou et al., 2019). A recently-published work found that landform element extraction by these classical approaches could vary significantly between moderate-resolution and high-resolution DEMs. Otherwise, aspect or direction, is viewed as an important element in image processing and pattern recognition. In comparison, the aspect in topography is defined as slope direction in some literature, which describes the downslope direction, or the direction toward which the stream flows on a land surface.

The reported findings inspire us continuing a research to explore the applicability and robustness of the aspect in landform element extraction on high-resolution DEMs. First, we present the study data and our presumptions regarding aspect for landform representation. Then, we generate the models of three classical method-system including fuzzy-based classification, feature descriptors and object-based segmentation. Based on the study data, we design several experiments to visually showed, quantitatively compared, and discussed the results of landform element extraction by three classical method-system, and their corresponding aspect-enhanced approaches. All experimental results could be used to test the effectiveness of aspect in improving the results of landform element extraction.

2 Study Area and Data

2.1 Study area

Fig. 1 uses topographic maps with contour lines to illustrate three study areas in America. Fig. 1A shows the first study area—the Meteor Crater and its surrounding areas. Meteor Crater locates in the northern Arizona. In this crater, the elevation of rims is relatively similar, composing as a circular-like crater. Meteor Crater is about 1720 m in average elevation and around 1200 m

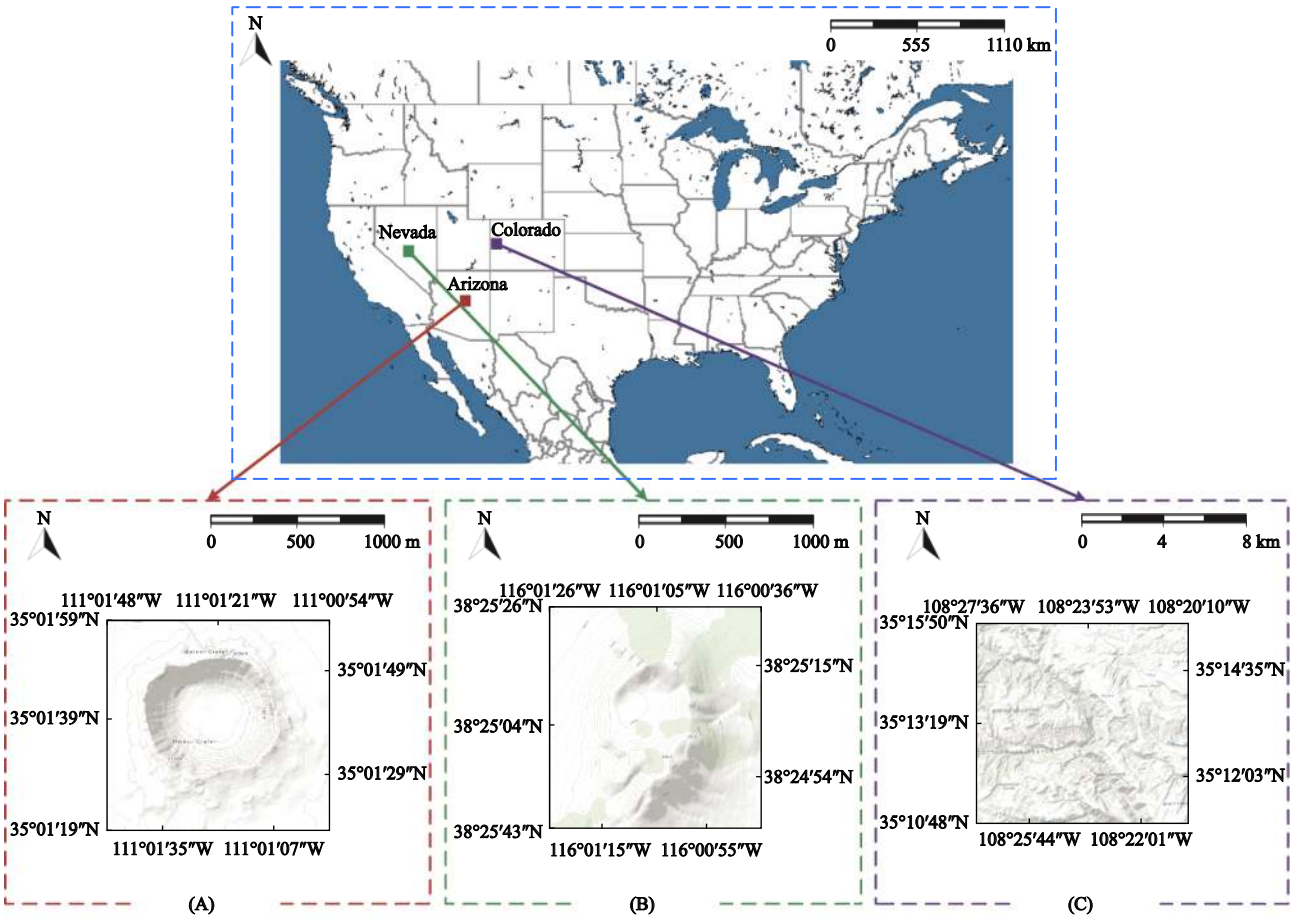

Fig. 1 Location of study areas in America and illustration of study area datasets

in average diameter. The bed of its center is about 1558 m deep. Meteor Crater is commonly known as one of the best-preserved meteorite crater on Earth.

Fig. 1B shows the second study area—a crater in the Lunar Crater National Natural Landmark in Nevada. The elevation of rims varies significantly in this crater. From the eastern rims to the wester ones, the elevation changes from 1935 m to 1866 m. This crater is about 1912 m in average elevation. The major axis and minor axis approximately follows the north-south direction and the east-west direction. These two axes are in around 720 m and 540 m.

We select these two craters as the study area based on two conditions. First, the rims of crater are ridgelines, and craters rims are visually recognizable on the high-resolution satellite image and DEM, making it easier to draw the ground truth ridgeline samples for evaluating the effectiveness of ridgeline extraction. Moreover, these two selected craters have different landforms. Elevation is approximately similar along the rims of the Meteor Crater. In comparison, the elevation changes substantially along the rims of the crater shown in Fig. 1B.

Fig. 1C shows the third study area, which locates in the northeastern area of Grand Junction, CO. We selected this region mainly covered by desert. This means that its terrestrial surface is smooth, without the effects of man-made facilities, trees and other non-terrain objects.

2.2 Data

For all study areas, we collected high-resolution resolution DEM datasets used for evaluating the impact of the aspect property for landform element extraction. The original DEM datasets for all study areas is 1 m in spatial resolution. For each original DEM, we respectively generated 2 m, 4 m and 8 m resolution DEMs accordingly.

The data dimensionality of the first and the second study areas is 2000 pixels by 2000 pixels and 1000 pixels by 1000 pixels, respectively. All these two DEM

datasets were accessed from OpenTopography (Krishnan et al., 2011), a cyberinfrastructure that provides high-resolution topography data and tools. Moreover, the data dimensionality of the third study areas is 10012 pixels by 10012 pixels. Because the coverage of this dataset is too large, we divided this dataset into 10 sub-datasets that have a dimensionality of 1000 pixels by 1000 pixels. The datasets were acquired from the National Elevation Dataset of the US Geological Survey (USGS NED).

3 Methods

3.1 Presumptions of aspect in landform representation

3.1.1 Rotation, scale and affine variance in aspect-based landform representation

Fig. 2 illustrates the cross-section profile of a terrain feature (ridge) after rotation, rescaling and affine transformation. Assume Points O and O′ respectively refer to the point of a ridgeline in the original DEM and in the DEM generated through rotation, rescaling and affine transformation. A and B, and A′ and B′ respectively are the neighboring pixels on the downslope sides of O and O′.

In Fig. 2A, the aspect difference between the downslope sides of Point A−Point O and the one of Point B−Point O is identical to the aspect difference between the downslope sides of Point A′−Point O′ and the one of Point B′ and Point O′. Fig. 2B illustrates the original and a scaled DEM generated through downscaling operation with Gaussian filter. Scale transformation happens when the same terrain object is represented by DEMs at different resolutions. The elevation, slope and curvature of Point O are not identical to those of Point O′. However, the aspect of Point O is the same as that of Point O′. This means that elevation, slope and curvature vary as the scale of DEM changes, but aspect is robust to scale variance. Fig. 2C illustrates the original and a new DEM generated by affine transformation with 2D (2-dimensional) geometric transformation. In the image or DEM processing, affine transformation is used to preserve points, straight lines, planes, and a set of parallel lines by linear way. Affine distortion might be observed in a raw DEM data without geometric rectification. In Fig. 2C, the slope and curvature of Point O are not identical to those of Point O′. Additionally, the elevation and aspect of Point O are the same as those of Point O′. Thus, only elevation and aspect are invariant to affine transformation.

Above all, aspect is not only able to represent the slope direction between two downslope sides of a landform element (e.g., ridge, valley, *etc*.) but is also robust to the variance of rotation, scaling and/or affine transformation. Moreover, although aspect alone can not quantitatively measure the extent of changes in elevation, it would be more useful for mapping a variety of landform elements than elevation difference, slope and curvature.

3.1.2 Aspect granularity

Resolution or scale plays an important role in landform representation (Deng, 2007; Drăguţ and Eisank, 2011; Li et al., 2016). Spatial resolution influences not only the accuracy of elevation values in a DEM data (Liu, 2008), but also the feature extraction results produced from its derivatives including curvature, slope and hillshade (Favalli and Fornaciai, 2017; Yang et al., 2020). Aside from spatial resolution and scale, the scale of aspect also impacts the representation of a landform. In this paper, we propose a new term called aspect granularity, or aspect scale, to define the fineness degree of aspect, which is shown in Fig. 3. The aspect granularity is defined as follows:

Aspect granularity: Aspect granularity refers to the minimum aspect difference available to be represented between two pixels in DEM. In the calculation, we set the aspect granularity in a range from greater or equal to 0° to less than 360°. When we meet 360°, we will

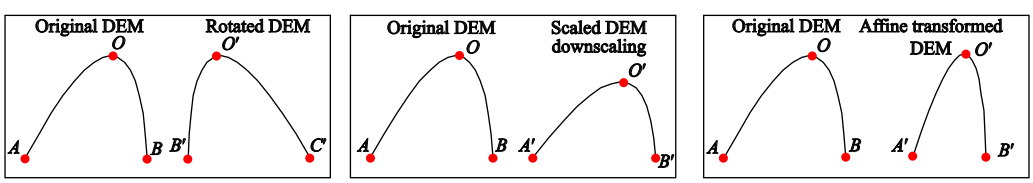

Fig. 2 Illustration on the robustness of aspect in rotation transformation (A); scaling transformation (B); affine transformation (C)

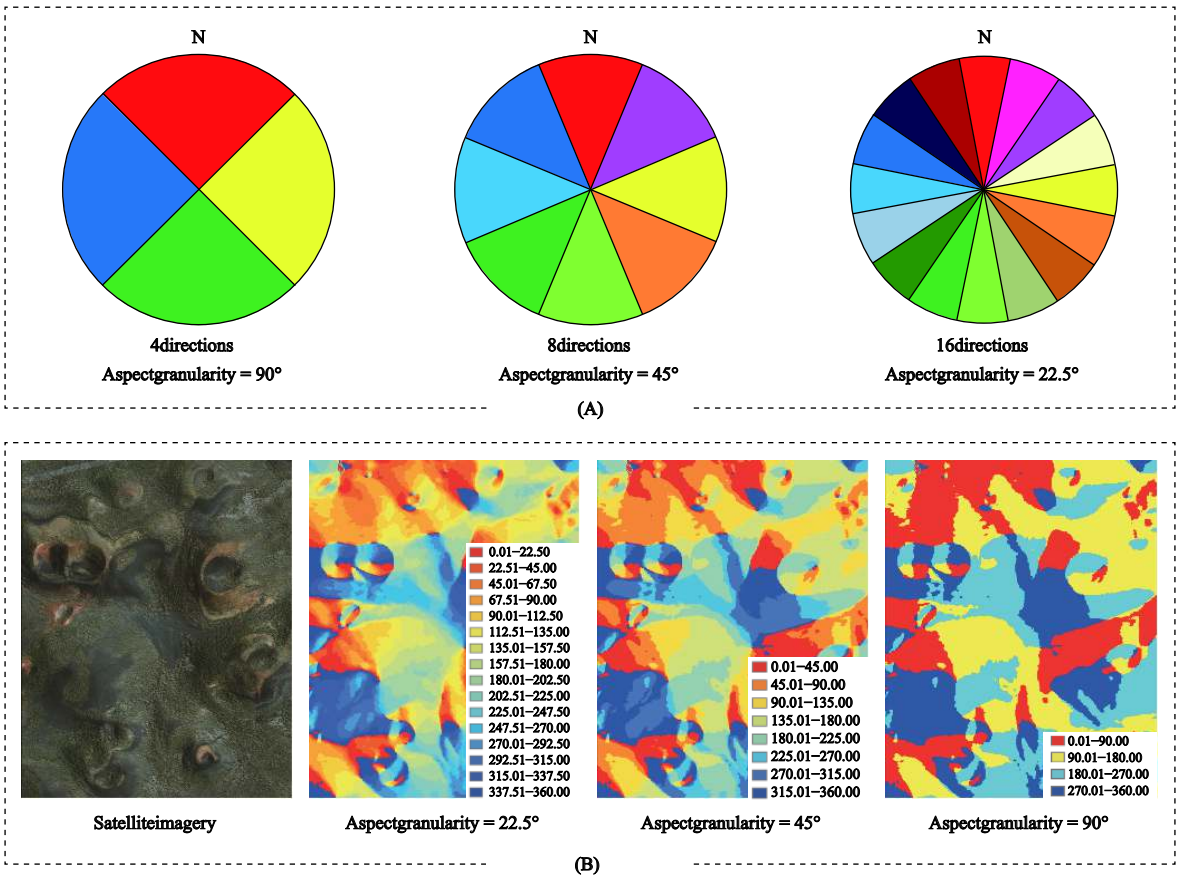

Fig. 3 Illustration of aspect granularity: theoretical aspect granularity (A); characteristics of land surface represented by different aspect granularities (B)

change it as 0°.

Fig. 3A shows the discretization scheme for the aspect attribute. When aspect granularity equals 90°, it supports the representation of landform by 4 directions. When aspect resolution is 45° or 22.5°, it can respectively represent landform with 8 directions. Moreover, shown in Fig. 3B, land surface is characterized differently for different aspect granularities. More details of terrain features and land surface are available by increasing aspect granularity. Similar to the spatial resolution of a DEM, aspect granularity also significantly impacts the representation of landform elements.

As shown in Fig. 3, aspect difference is sensitive to the elevation variation of the downsides of a landform element (e.g., ridge and valley point). Thus, the bigger aspect granularity enables the representation of fine-detailed elevation variation, which means that the bigger aspect granularity could represent more details of land surface. However, the bigger aspect granularity also might raise the possibility of the existence of noises. Thus, appropriate aspect granularity is also critical to well-landform element extraction, and even landform characterization. To our knowledge, 45° is generally appropriate for around 10 m DEM-based landform element extraction, and 22.5° is generally appropriate for 1 m DEM-based landform element extraction.

3.2 Aspect enhanced curvature-based fuzzy classification for landform element extraction

Fuzzy classification aims to classifying data into various fuzzy sets or semantic categories using fuzzy propositional functions. Fuzzy classification is useful to address a problem that contains values ranging from completely true to completely false. In landform element extraction, the techniques of fuzzy sets, fuzzy logic and fuzzy classification have been used to determine the propositional conditions for classifying land surface into predefined landform elements (Jiang et al., 2018; Zhu et al., 2018).

Previous methods (Jiang et al., 2018; Zhu et al., 2018) implemented fuzzy classification to characterize landforms based on the curvature map. We used this fuzzy

classification to extract ridges and valleys based on curvature map (curvature-based fuzzy classification) and the map fusing aspect and curvature (aspect enhanced curvature-based fuzzy classification), respectively. There includes two sequential parts.

(1) As shown in Fig. 4A, both curvature-based fuzzy classification and aspect enhanced curvature-based fuzzy classification follows the procedure described be-

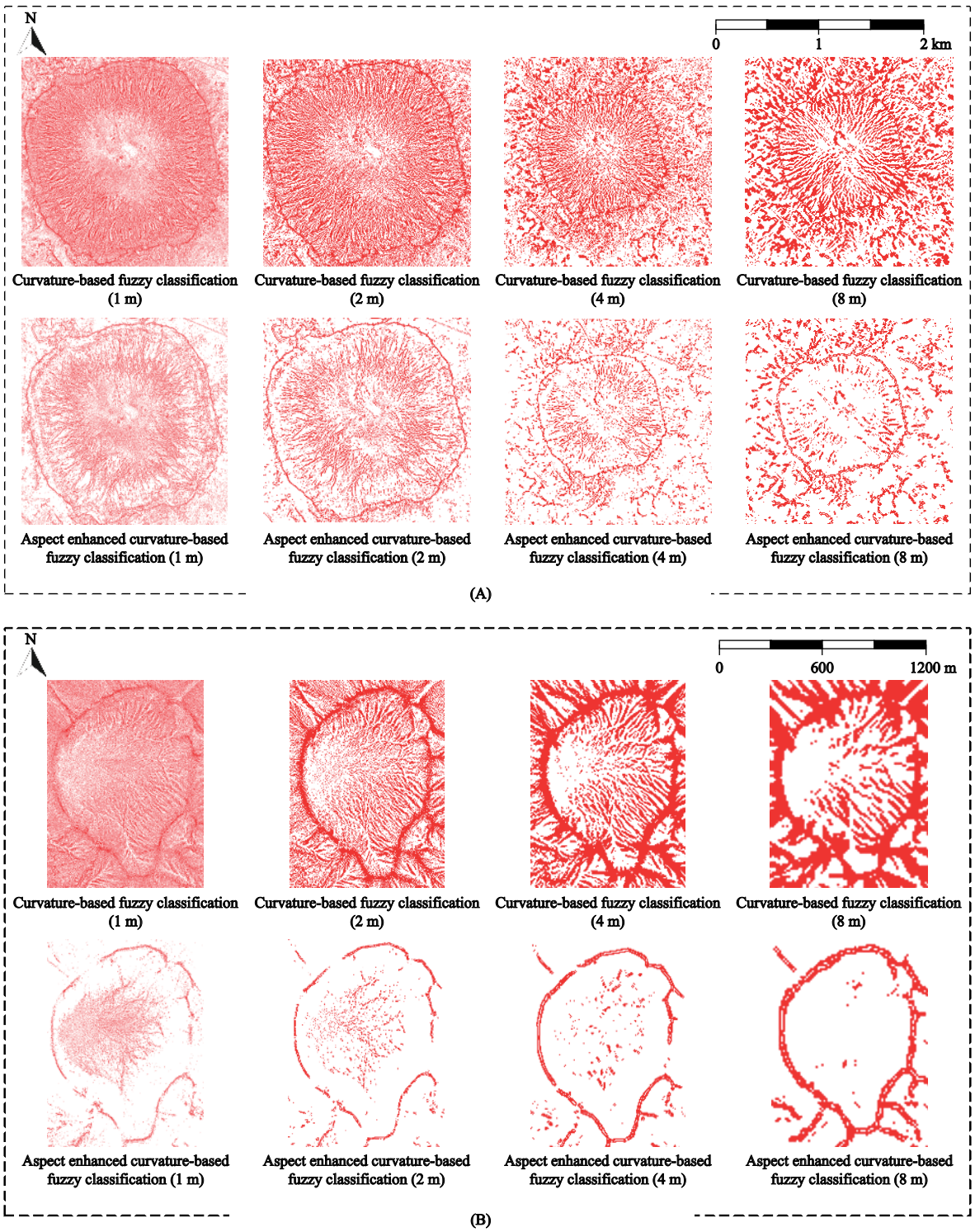

Fig. 4 The result comparison of curvature-based and aspect enhanced curvature-based fuzzy classification in study areas shown in Fig. 1A (A) and Fig. 1B (B)

low:

Assume a pixel in the aspect map is $A(x_0, y_0)$, where (x_0, y_0) denotes the location of this pixel.

Step 1. Computing the aspect difference between $A(x_0, y_0)$ and its neighboring pixels in eight directions, which are denoted by AD_{dir}, where dir refers to the index of eight directions.

Step 2. Based on two AD_{dir} in the opposite directions, for example, the AD_{dir} in east and west (AD_{east} and AD_{west}), we label this pixel as 1 if the following preconditions are satisfied:

if one of these two AD_{dir} is greater than 22.5

if another of these two AD_{dir} is less than 22.5

For example, if AD_{east} is greater than 22.5 and AD_{west} is less than 22.5, we label $A(x_0, y_0)$ as 1. Since the resolution of DEM used for experiment is 1m, we set the granularity of aspect difference as 22.5.

Step 3. If the condition in Step 2 is not satisfied, we label this pixel as 0.

Step 4. Generate a new map including all labeled pixels.

(2) Then, we respectively conduct the curvature-based fuzzy classification and aspect enhanced curvature-based fuzzy classification.

The structure of curvature-based fuzzy classification for ridge and valley extraction is shown as follows:

$$f(x_0, y_0) = \begin{cases} 1, C(x_0, y_0) \in [\theta 1, +\infty) \\ -1, C(x_0, y_0) \in (-\infty, \theta 2] \\ 0, C(x_0, y_0) \in (\theta 2, \theta 1) \end{cases} \tag{1}$$

where $f(x_0, y_0)$ is the fuzzy propositional function for determining whether one pixel in the coordinate (x_0, y_0) of a DEM belongs to a ridge, valley or non-terrain feature, $C(x_0, y_0)$ is the mean curvature value of this pixel and $\theta 1$ and $\theta 2$ are curvature thresholds for ridges and valleys. When the curvature value of a pixel is greater than $\theta 1$, this pixel is classified as a ridge. When the curvature value of a pixel is lower than $\theta 2$, this pixel is classified as a valley. Otherwise, this pixel would be classified as a non-ridge or valley pixel.

The following expression shows aspect enhanced curvature-based fuzzy classification for ridge and valley extraction, where $\theta 1$ and $\theta 2$ are two thresholds for determining ridgelines and valley lines, and $AD_+(x_0, y_0)$ and $AD_-(x_0, y_0)$ refer to the aspect difference of $A(x_0, y_0)$ in two opposite directions:

$$f(x_0, y_0) = \begin{cases} 1, AD_+(x_0, y_0) \geq 22.5 \text{ and } AD_-(x_0, y_0) < \\ \quad 22.5 \text{ and } C(x_0, y_0) \in [\theta 1, +\infty) \\ -1, AD_+(x_0, y_0) \geq 22.5 \text{ and } AD_-(x_0, y_0) < \\ \quad 22.5 \text{ and } C(x_0, y_0) \in (-\infty, \theta 2] \end{cases} \tag{2}$$

3.3 Aspect enhanced elevation-based feature descriptor for landform element extraction

Local features of computer vision (Li and Allinson, 2008) focus on discovering the salient features (or points of interesting) as the features of an image object at various scales and rotations. Some algorithms that were successfully used in computer vision, such as local binary pattern (LBP), image pyramid and so on, have implemented into landform element extraction.

This paper uses the LBP to conduct pixel-level terrain analysis based on elevation (Jasiewicz and Stepinski, 2013) and aspect, respectively. In a 3-pixel by 3-pixel window, the center pixel has eight neighboring pixels. The method compared this center pixel and its neighboring pixel in each direction with ternary patterns including 1, 0 and –1. The ternary patterns are acquired by the following equation,

$$LBP(p_0 - p_a) = \begin{cases} 1, p_0 - p_a > 0 \\ 0, p_0 - p_a = 0 \\ -1, p_0 - p_a < 0 \end{cases} \tag{3}$$

where p_0 and p_a respectively refers to the value of the center pixel and its neighboring pixel in one of eight directions in the 3 × 3 window.

Thus, the LBP of a pixel (the center pixel) would compose of eight values. Unlike the pattern defined by computer vision, Jasiewicz and Stepinski (2013) ignored the sequence of these eight neighboring directions, and predefine 10 patterns for a variety of landform elements, including flat and slope, peak and pit, ridge and valley, shoulder and footslope, and spur and hollow.

3.4 Aspect enhanced curvature-based segmentation for landform element extraction

The differences between pixel-based and object-based data analysis have been discussed for more than a decade. Pixel alone can not represent the characteristics of a region in a DEM. The object-based strategy aims to cluster or group similar pixels into a superpixel. Based on the literature (Whiteside et al., 2011; Liu et al.,

2017), the object-based approach is expected to have a better capability of mapping landforms from high-resolution DEMs. First, object-based segmentation can overcome the negative influence of noises like 'salt-pepper noise', 'salt-pepper noise' mainly originates from the detailed roughness of the land surface represented by a high-resolution DEM. Unlike low- and moderate resolution DEMs, which describe a relatively smooth surface, the details of roughness of land surface (e.g., stones, small convex and concave) in a high-resolution DEM provides might become 'salt-pepper noise'. Moreover, object-based segmentation supports landform element extraction based on the contextual information, such as texture, pattern, structure and so on.

In this experimental subsection, a cutting-edge object-based segmentation called simple linear iterative clustering (SLIC) is applied to segment a 1 m DEM, 1m curvature map and 1m aspect map, respectively. SLIC (Achanta et al., 2012) clusters the pixels as a superpixel (or object) through measuring the distance over spatial space and intensity (color) difference. In SLIC, the space that includes color space and spatial space is represented as (L, A, B, X, Y), where L, A and B denote three channels of Lab color space, and X and Y denote the horizontal and vertical dimensions of the image. Because a DEM, curvature map, or aspect map includes only one channel, the space of SLIC based on elevation, curvature, or aspect is changed as $(attr_{\sigma,X,Y})$, where σ refers to one of the three attributes: elevation, curvature or aspect. X and Y denote the horizontal and vertical dimensions of the data. Then, the function of SLIC is shown as follows:

$$SLIC(attr_{\sigma,X,Y}, g, \theta) \tag{4}$$

where $attr_{\sigma,X,Y}$ is the result of normalizing the original DEM, curvature map, or aspect map ($attr_{\sigma}$). In other words, the original value range of $attr_{\sigma,X,Y}$ is transformed into the value range of (0–1) in the $attr_{\sigma,X,Y}$. g denotes the sigma of the Gaussian filter, which is used to control the degree of smoothing. In this work, the value of g is 1. Moreover, to avoid missing the substructures that belong to a landform object, a smaller scale parameter value (θ) is given to generate a result that has a bigger possibility of including more small objects.

The following equation shows the distance that measures the difference between two pixels (D_{total}) in the SLIC segmentation:

$$D_{\text{total}} = D_z + \frac{\theta}{\sqrt{N}} \times D_{xy} \tag{5}$$

where D_{total} refers to the final distance that measures the difference of two pixels. D_z refers to the distance of attribute (e.g., elevation, curvature, or aspect) between two pixels, D_{xy} refers to the spatial distance of two pixels. θ denotes the ratio between spatial distance and attribute difference (elevation, curvature or aspect). The bigger θ leads to generating a result that including large landform objects, and vice versa. N denotes the approximate number of superpixels after segmentation. Moreover, D_{attr} and D_{xy} are obtained by the following equation:

$$\begin{cases} D_z = \sqrt{D_{\text{attr}}^2 + D_{\text{attr}}^2 + D_{\text{attr}}^2} \\ D_{xy} = \sqrt{(D_x)^2 + (D_y)^2} \end{cases} \tag{6}$$

where D_{attr} refers to the difference of attribute (elevation, curvature or aspect) between two pixels. D_x and D_y denote the distance between two pixels in horizontal and vertical dimensions, respectively.

4 Experiments and Discussion

4.1 Comparison of curvature-based and aspect enhanced curvature-based fuzzy classification

Fig. 4 shows the results of ridgeline (crater rim) extraction using mean curvature-based fuzzy classification and aspect enhanced curvature-based fuzzy classification. The threshold of mean curvature was 0.01, because it enabled extracting a majority of the crater boundary. We generated the extraction results based on four groups of high-resolution DEMs (1 m, 2 m, 4 m and 8 m resolution DEM) by each method. The red parts are the extracted ridgelines. In the results of Fig. 4A and Fig. 4B, mean curvature-based fuzzy classification included a lot of false positive results, making it impossible to derive the true boundaries of the two craters. Additionally, a majority of the extracted ridgelines were tiny and incomplete. In comparison, the boundaries of two craters in the results shown in Fig. 4A and Fig. 4B are much clearer, proving that the fuzzy classification fusing aspect and mean curvature held better capability of extracting ridgelines on the high-resolution DEM.

Moreover, mean curvature-based fuzzy classification generally produces proper noises in the ridgeline extrac-

tion result based on the lower resolution DEMs. This means that the detailed roughness of land surface available in high-resolution DEMs (1 m, 2 m, 4 m and 8 m) would result in many non-ridgelines being extracted by mean curvature alone. In the results derived from Fig. 4A, the crater rims were not clear by integrating aspect difference. However, in the results derived from Fig. 4B, by integrating aspect difference, the crater rims were much more easily distinguished from their context. If the landform varied mild, like the crater in Fig. 4A, curvature alone might be appropriate. Otherwise, for the landform like the crater in Fig. 4B that had significant changes in elevation and slope, the approach integrating aspect difference and mean curvature could handle noises and the features being similar to ridgelines available in the high-resolution DEM.

Above of all, the results in Fig. 4 proved that the fuzzy classification—commonly used approach for moderate resolution DEM—could be competent for high-resolution DEM while integrating aspect.

4.2 Comparison of elevation-based feature descriptor and aspect enhanced elevation-based feature descriptor

Fig. 5 shows the results of crater rim (ridgeline) extraction using elevation-based LBP and aspect enhanced elevation-based LBP. The threshold of elevation and aspect are 0.06 and 22.5, respectively. The red parts are the extracted ridgelines. We generated the extraction based on the 1 m, 2 m, 4 m and 8 m resolution DEM by each method. In the results of Fig. 5A and Fig. 5B, elevation-based LBP produced much more nonlinear ridgelines than aspect enhanced elevation-based LBP. Moreover, the ridgelines in the interior part of the crater were not extracted by elevation-based LBP. This is because a majority of ridgelines in the interior part of the Meteor Crater were only extracted by platform curvature. For the second crater, elevation-based LBP and aspect enhanced elevation-based LBP generated similar results for extracting the ridgelines. In this crater, the slopes of partial ridgelines (rims) in the interior are very smooth, making them impossible to be characterized by elevation difference and aspect difference.

Moreover, many branches were observed in the result of crater rim extraction using elevation-based LBP. The elevation-based LBP reported by Jasiewicz and Stepinski was tested on a 30 m DEM. On this occasion, crater rims (ridgelines) have a distinct elevation difference compared with their context. Thus, the elevation-based LBP could generate a result better than the one generated by aspect-enhanced LBP. However, when the detailed roughness of land surface was available in a high-resolution DEM, the ridge or crater rimes could not be distinguished well by elevation difference. Elevation-based LBP is incompetent to predefine precise pattern templates for representing complicated landforms. Otherwise, the total number of ridgelines (crater rimes) extracted by aspect enhanced elevation-based LBP still seemed insufficient. This means that the patterns of specific landforms might be very difficult well defined on the high-resolution DEM.

4.3 Comparison of elevation-based segmentation, curvature-based segmentation and aspect enhanced curvature-based segmentation

Fig. 6 shows the results of crater boundary (ridgeline) extraction using elevation-based SLIC, curvature-based SLIC and aspect enhanced curvature-based SLIC, respectively. We generated the extraction based on the 1 m, 2 m, 4 m and 8 m resolution DEM by each method. The approximate number of segmentations and Gaussian scales used for segmentation is 3000 and 2. In the results of Fig. 6A and Fig. 6B, few lines extracted were true ridgelines. In the results of Fig. 6A and Fig. 6B, although the contour of these two craters was slightly observed, only few lines extracted were true ridgelines. Moreover, the rims of these two craters are impossible to be recognized from the results by elevation-based segmentation and curvature-based segmentation. These lines belonging to the crater rims seem impossible to separate from other lines extracted without manual interpretation.

In comparison, the contour of these two craters was much more recognizable to a greater degree in the results of Fig. 6A and Fig. 6B. Similar to the example shown in Fig. 2, the contour of landform, or the ridgeline, or the crater rim was easily mapping by aspect difference. Otherwise, we also found that the segmentation results had few difference on 4 m and 8 m resolution DEM, respectively.

4.4 Result analysis and discussion

Considering that the ground truth datasets were not

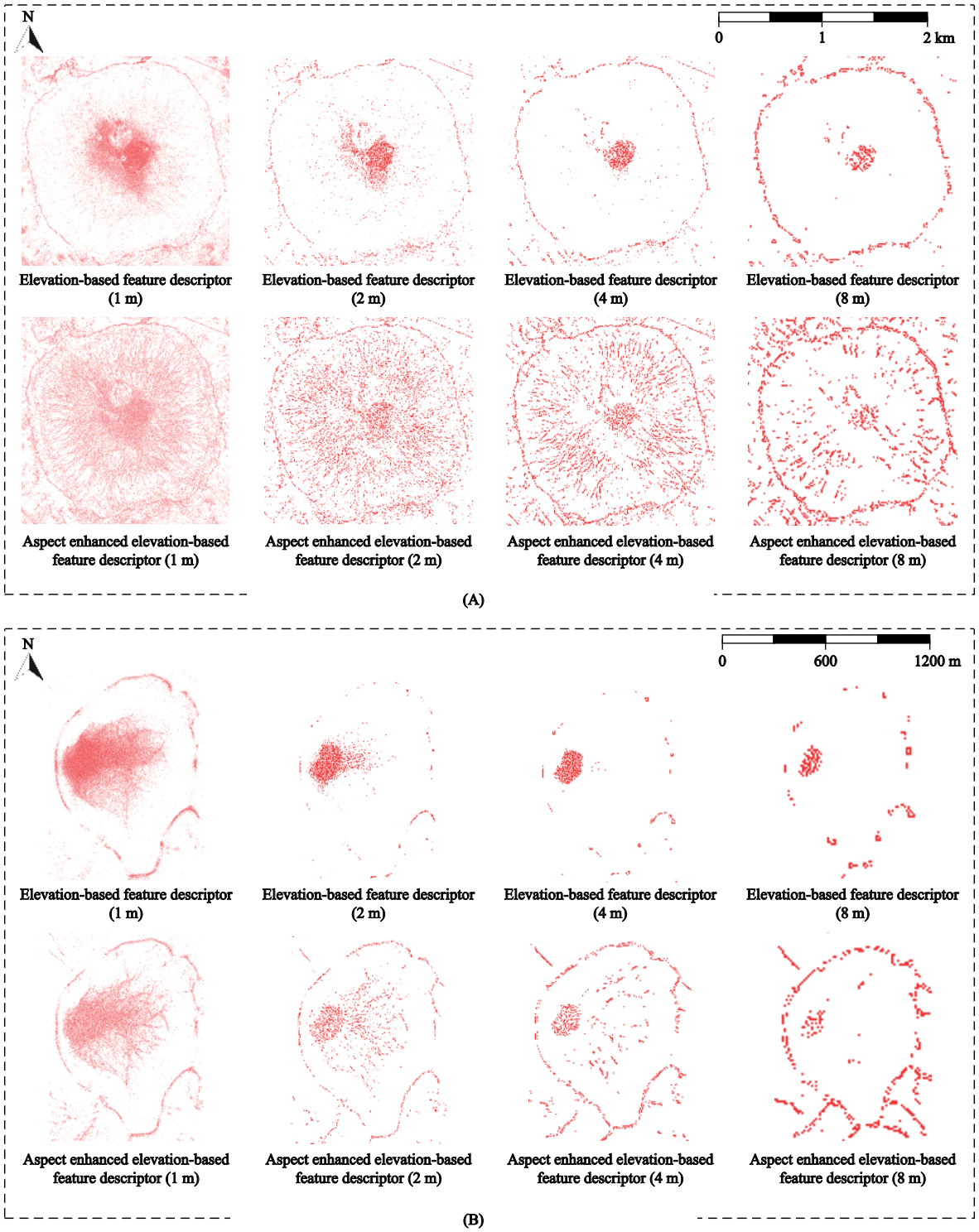

Fig. 5 The result comparison of elevation-based feature descriptor and aspect enhanced elevation-based feature descriptor in study areas shown in Fig. 1A (A) and Fig. 1B (B)

available, we visually drawn the referenced crater rims based on the satellite images and mean curvature map of these two craters. Since the surface of these two craters is very toughly recognizable from the high-resolution DEM, we set the width of the visually-generated rater rims as 5 m. Any extracted pixels being inside of the crater rims were labeled as true extracted pixel.

Besides the visual-based comparisons shown in Fig. 4

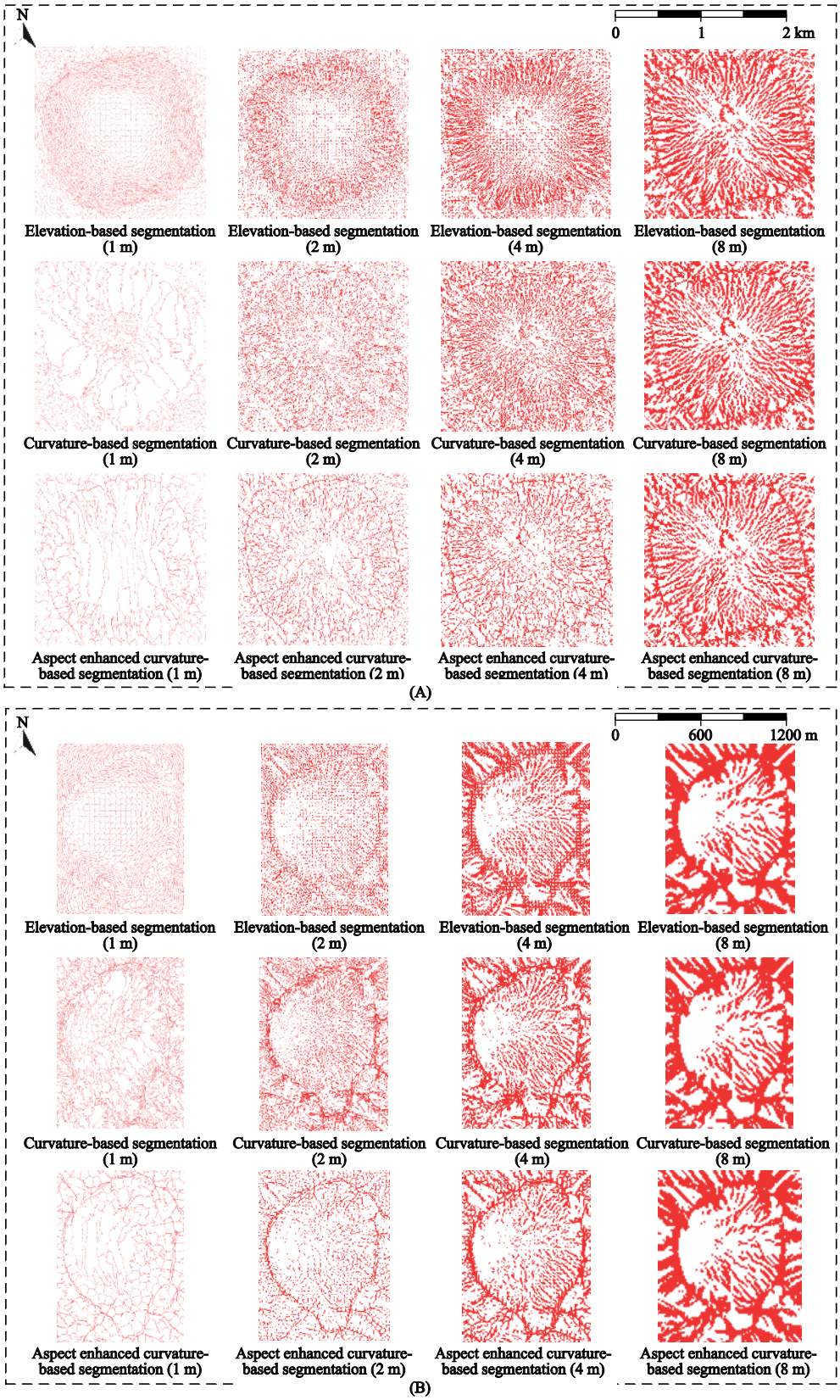

Fig. 6 The result comparison of elevation-based segmentation, curvature-based segmentation and aspect enhanced curvature-based segmentation in study areas shown in Fig. 1A (A) and Fig. 1B (B)

to Fig. 6, we use precision (P) and recall (R) to quantitatively measure the results by different methods.

$$\begin{cases} P = \dfrac{TP}{TP+FP} \\ R = \dfrac{TP}{TP+FN} \end{cases} \tag{7}$$

where TP, FN and FP respectively refers to the total amount of true positive extracted pixels, the total amount of false negative extracted pixels, and false positive extracted pixels. Precision measures the ratio between correctly extracted pixels and all extracted pixels, or how many extracted pixels are true topographical features. Otherwise, recall measures the ratio between correctly extracted pixels and all true pixels, or how many topographical features are extracted. Table 1 to Table 3 list the precision and recalls for each result shown in Fig. 4 to Fig. 6.

In comparison to the results generated by mean curvature (Jiang et al., 2018; Zhu et al., 2018), joining the fuzzy set of aspect difference can effectively enhance defining the characteristics of ridgelines and valleylines based on the high-resolution DEM. The results generated by mean curvature-based fuzzy classification might include many true negative errors because ridgelines, as well as shoulders would be extracted. When the detailed roughness of land surface was available in a high-resolution DEM, a ridge and a shoulder, or a valley and a footslope, might have approximately similar curvature values. In this case, both the shoulder and ridge would possible be extracted using the mean curvature alone. In some cases, the curvature of a ridge point or a valley point was even smaller than a shoulder point or a footslope point. Under this condition, only the shoulder and footslope would be extracted by mean curvature alone.

The feature descriptor method (LBP) proposed by Jasiewicz and Stepinski (2013) was significance of extracting main landform elements, however, we found that its performance varied considerably when using different DEM derivatives. By integrating aspect difference, the new 2D template of LBP can better define the complicated context of a valleyline or ridgeline. Thus, the LBP integrating aspect difference and elevation could generate better extraction results of landform elements than the elevation-based LBP from the high-resolution DEMs. Otherwise, many broken lines also existed in the extraction results. This might be because the limits of pixel-level approach in extracting landform elements from high-resolution DEM. The land surface on the 1 m DEM is much more complicated than and significantly different from the 30 m DEM. This proves that it is challenging to predefine the template (or pat-

Table 1 Quantitative statistical analysis and comparison of curvature-based and aspect enhanced curvature-based fuzzy classification

Figure	Resolution / m	Method	Precision	Recall
Fig. 4A	1	Curvature-based fuzzy classification	0.1459	0.8822
		Aspect-enhanced curvature-based fuzzy classification	**0.3272**	**0.9174**
	2	Curvature-based fuzzy classification	0.1676	0.9170
		Aspect-enhanced curvature-based fuzzy classification	**0.3651**	**0.9347**
	4	Curvature-based fuzzy classification	0.1901	0.9535
		Aspect-enhanced curvature-based fuzzy classification	**0.4235**	**0.9589**
	8	Curvature-based fuzzy classification	0.2121	0.9703
		Aspect-enhanced curvature-based fuzzy classification	**0.5371**	**0.9784**
Fig. 4B	1	Curvature-based fuzzy classification	0.1224	0.8036
		Aspect-enhanced curvature-based fuzzy classification	**0.3272**	**0.7562**
	2	Curvature-based fuzzy classification	0.1652	0.9221
		Aspect-enhanced curvature-based fuzzy classification	**0.4520**	**0.8065**
	4	Curvature-based fuzzy classification	0.2830	0.9689
		Aspect-enhanced curvature-based fuzzy classification	**0.5898**	**0.8927**
	8	Curvature-based fuzzy classification	0.4033	0.9851
		Aspect-enhanced curvature-based fuzzy classification	**0.8572**	**0.9560**

Table 2 Quantitative statistical analysis and comparison of elevation-based feature descriptor and aspect enhanced elevation-based feature descriptor

Figure	Resolution / m	Method	Precision	Recall
Fig. 5A	1	Elevation-based LBP	0.3051	0.7727
		Aspect-enhanced elevation-based LBP	**0.1716**	**0.8891**
	2	Elevation-based LBP	0.3671	0.8105
		Aspect-enhanced elevation-based LBP	**0.2163**	**0.8836**
	4	Elevation-based LBP	0.4682	0.8330
		Aspect-enhanced elevation-based LBP	**0.2571**	**0.9072**
	8	Elevation-based LBP	0.5948	0.8581
		Aspect-enhanced elevation-based LBP	**0.3891**	**0.9311**
Fig. 5B	1	Elevation-based LBP	0.2908	0.4336
		Aspect-enhanced elevation-based LBP	**0.3251**	**0.5296**
	2	Elevation-based LBP	0.2537	0.2137
		Aspect-enhanced elevation-based LBP	**0.3233**	**0.4607**
	4	Elevation-based LBP	0.2175	0.1505
		Aspect-enhanced elevation-based LBP	**0.2574**	**0.3856**
	8	Elevation-based LBP	0.2409	0.1755
		Aspect-enhanced elevation-based LBP	**0.5762**	**0.7147**

Note: LBP is feature descriptor method

Table 3 Quantitative statistical analysis and comparison of elevation-based segmentation, curvature-based segmentation and aspect enhanced curvature-based segmentation

Figure	Resolution / m	Method	Precision	Recall
Fig. 6A	1	Elevation-based segmentation	0.0729	0.3561
		Curvature-based segmentation	0.0232	0.0895
		Aspect enhanced curvature-based segmentation	**0.1328**	**0.7181**
	2	Elevation-based segmentation	0.1009	0.3788
		Curvature-based segmentation	0.0526	0.1450
		Aspect enhanced curvature-based segmentation	**0.1961**	**0.7615**
	4	Elevation-based segmentation	0.1323	0.3971
		Curvature-based segmentation	0.0709	0.2016
		Aspect enhanced curvature-based segmentation	**0.2217**	**0.8271**
	8	Elevation-based segmentation	0.1510	0.4852
		Curvature-based segmentation	0.0934	0.3379
		Aspect enhanced curvature-based segmentation	**0.2518**	**0.8661**
Fig. 6B	1	Elevation-based segmentation	0.0837	0.0505
		Curvature-based segmentation	0.1071	0.1826
		Aspect enhanced curvature-based segmentation	**0.3590**	**0.7644**
	2	Elevation-based segmentation	0.1108	0.8772
		Curvature-based segmentation	0.1363	0.8256
		Aspect enhanced curvature-based segmentation	**0.4244**	**0.9371**
	4	Elevation-based segmentation	0.3637	0.9478
		Curvature-based segmentation	0.4170	0.8966
		Aspect enhanced curvature-based segmentation	**0.4426**	**0.9556**
	8	Elevation-based segmentation	0.4882	0.9675
		Curvature-based segmentation	0.4765	0.9632
		Aspect enhanced curvature-based segmentation	**0.5103**	**0.9660**

tern) to precisely represent the complicated elevation variations of land surface on high-resolution DEMs.

For multi-segmentation, elevation-based segmentation and curvature-based segmentation basically might not be used for extracting ridgelines on the high-resolution DEM. Both of these two approaches only detect the edges that carry significant elevation variation, a majority of which belong to shoulders rather than ridges. Moreover, based on a high-resolution DEM, the segmentation algorithm would be very sensitive to the elevation and curvature difference between two side of a ridgeline or a valleyline. Last but not least, the two sides of a ridgeline would carry a distinct aspect difference, which might be not in such way for a shoulder, or a footslope. Thus, by integrating aspect feature, the context of ridgelines and the representation of complicated landform are much more discernable in the high-resolution DEMs. This explain why aspect enhanced curvature-based segmentation outperforms the elevation-based and curvature-based segmentation.

Moreover, in Fig. 7, we present the significance of aspect through the curvature map and aspect map of Meteor Crater. Landform elements including ridge, valley, shoulder and foot-slope seem impossible to be precisely

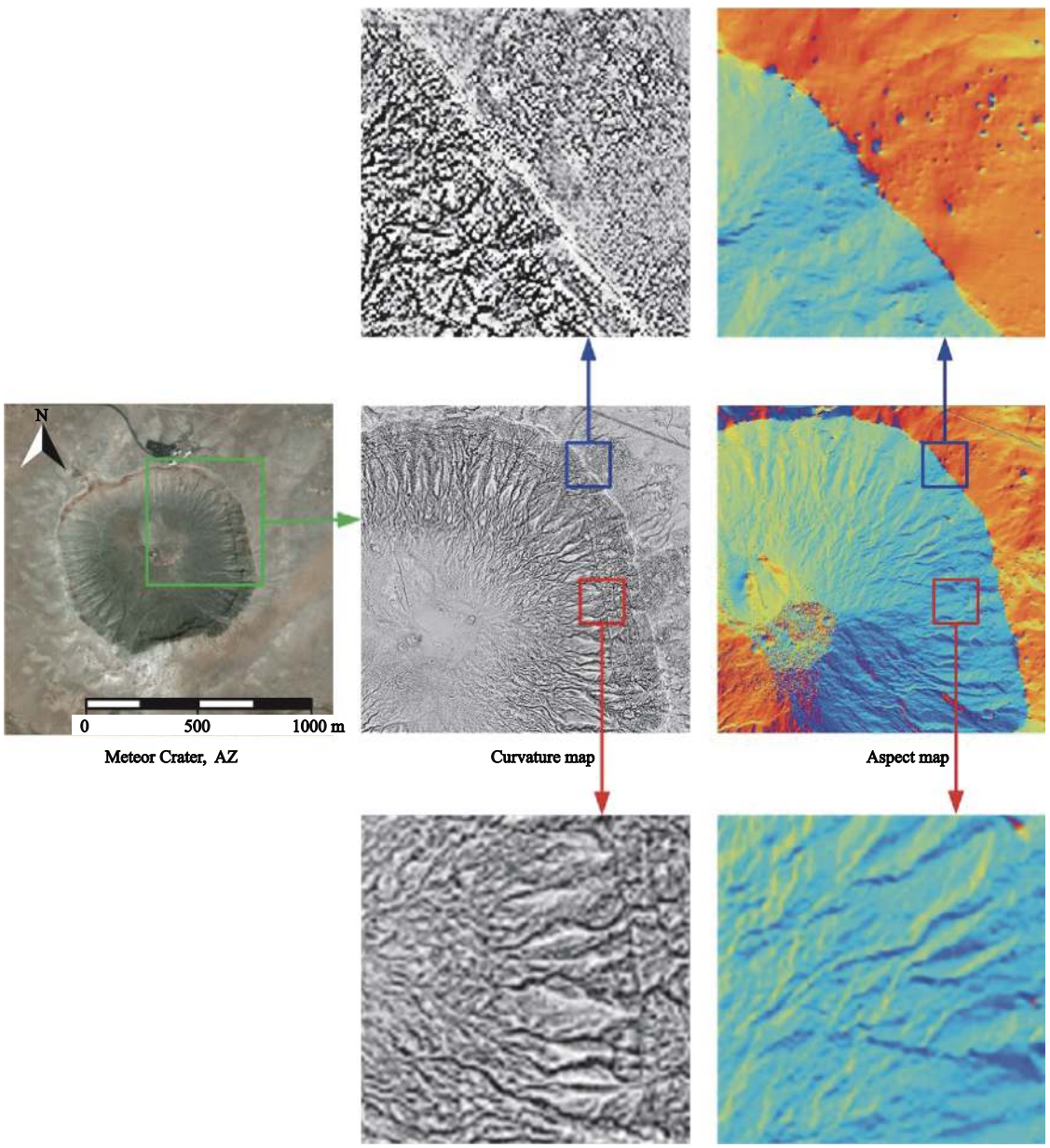

Fig. 7 Illustration on curvature-based and aspect-based terrain feature representation in Meteor Crater, Arizona, America

mapping from the high-resolution curvature map, which is created by the mean curvature calculation tool in ArcGIS. Otherwise, the detailed boundary and micro-topography of Meteor Crater is much more discernable in the aspect map and its partially enlarged view.

Last but not least, through the experimental results, we found that the appropriate aspect granularity for topographical feature extraction might vary according to the spatial resolution of high-resolution DEM. As shown in Figs. 4–6 and Tables 1 to 3, the appropriate granularity of aspect relies on the scale (or the spatial resolution) of topographical features. Generally speaking, regarding the adaptive aspect granularity, the aspect granularity—22.5 relatively fit for 1–5 m high-resolution DEM, and the aspect granularity—45 relatively fit for 5–m high-resolution DEM. For the DEM that has a resolution higher than 1 m, 11.25 is relatively the appropriate aspect granularity. Since the higher resolution DEM represents more complicated land surface, we assume that the bigger aspect granularity would be appropriate for analyzing the more complicated surface. In other words, the aspect granularity is proportion to the scale of land surface and the resolution of DEM in topographical feature extraction.

5 Conclusions

The value of the high-resolution data lies in the high-precision feature information. The fine-detailed landform element extraction is thus the basis of high-fidelity application of the high-resolution DEMs. In confront of the difficulty of the existing approaches in maintaining the accuracy of fine-detailed landform element on the high-resolution DEM, this paper focus on comprehensively examining the significance of aspect in topography for improving the performance of classical approaches in landform element extraction.

In this paper, we compare the extraction results based on four groups of high-resolution DEMs (1 m, 2 m, 4 m and 8 m resolution DEM). According to the extraction results including crater rims by fuzzy classification, feature descriptor-based detection, and object-based segmentation, aspect can enhance the performance of these classical approaches in terms of landform element extraction on high-resolution DEMs. In the future, aspect could be an important attribute for landform characterizations based on high-resolution DEMs. Integrating aspect and other elevation derivatives (e.g., curvature, hillshade, slope, *etc*.) is expected to support accurate landform element extraction and visualization.

References

Achanta R, Shaji A, Smith K et al., 2012. SLIC superpixels compared to state-of-the-art superpixel methods. *IEEE Transactions on Pattern Analysis and Machine Intelligence*, 34(11): 2274–2282. doi: 10.1109/TPAMI.2012.120

Arundel S T, Bulen A N, Adkins K F et al., 2018. Assimilation of the National Elevation Dataset and launch of the 3D elevation program through the USGS spatial data infrastructure. *International Journal of Cartography*, 4(2): 129–150. doi: 10.1080/23729333.2017.1288533

Asselen S, Seijmonsbergen A C, 2006. Expert-driven semi-automated geomorphological mapping for a mountainous area using a laser DTM. *Geomorphology*, 78(3–4): 309–320. doi: 10.1016/j.geomorph.2006.01.037

Chaplot V, Darboux F, Bourennane H et al., 2006. Accuracy of interpolation techniques for the derivation of digital elevation models in relation to landform types and data density. *Geomorphology*, 77(1−2): 126–141. doi: 10.1016/j.geomorph.2005.12.010

Deilami K, Hashim M, 2011. Very high resolution optical satellites for DEM generation: a review. *European Journal of Scientific Research*, 49(4): 542–554.

Deng Y X, 2007. New trends in digital terrain analysis: landform definition, representation, and classification. *Progress in Physical Geography*, 31(4): 405–419. doi: 10.1177/0309133307081291

Dikau R, 1989. The application of a digital relief model to landform analysis in geomorphology. In: Raper J (eds.). *Three Dimensional Applications in Geographical Information Systems*. London: Taylor and Francis Press, 51–77.

Drăguţ L, Blaschke T, 2006. Automated classification of landform elements using object-based image analysis. *Geomorphology*, 81(3−4): 330–344. doi: 10.1016/j.geomorph.2006.04.013

Drăguţ L, Eisank C, 2011. Object representations at multiple scales from digital elevation models. *Geomorphology*, 129(3−4): 183–189. doi: 10.1016/j.geomorph.2011.03.003

Ehsani A H, Quiel F, 2008. Geomorphometric feature analysis using morphometric parameterization and artificial neural networks. *Geomorphology*, 99(1−4): 1–12. doi: 10.1016/j.geomorph.2007.10.002

Evans I S, 2012. Geomorphometry and landform mapping: what is a landform? *Geomorphology*, 137(1): 94–106. doi: 10.1016/j.geomorph.2010.09.029

Favalli M, Fornaciai A, 2017. Visualization and comparison of DEM-derived parameters: application to volcanic areas. *Geomorphology*, 290: 69–84. doi: 10.1016/j.geomorph.2017.02.029

Jasiewicz J, Stepinski T F, 2013. Geomorphons—a pattern recog-

nition approach to classification and mapping of landforms. *Geomorphology*, 182: 147–156. doi: 10.1016/j.geomorph.2012.11.005

Jiang L, Ling D Q, Zhao M W et al., 2018. Effective identification of terrain positions from gridded DEM data using multimodal classification integration. *ISPRS International Journal of Geo-Information*, 7(11): 443. doi: 10.3390/ijgi7110443

Krishnan S, Crosby C, Nandigam V et al., 2011. OpenTopography: a services oriented architecture for community access to LIDAR topography. In *Proceedings of the 2nd International Conference on Computing for Geospatial Research & Applications* (*COM.Geo* '11). Association for Computing Machinery, New York, USA, Article 7: 1–8. doi: https://doi.org/10.1145/1999320.1999327

Li J, Allinson N M, 2008. A comprehensive review of current local features for computer vision. *Neurocomputing*, 71(10-12): 1771–1787. doi: 10.1016/j.neucom.2007.11.032

Li J Z, Liu Y M, Mo C H et al., 2016. IKONOS image-based extraction of the distribution area of *Stellera chamaejasme* L. in Qilian county of Qinghai province, China. *Remote Sensing*, 8(2): 148. doi: 10.3390/rs8020148

Liu Kai, Ding Hu, Tang Guoan et al., 2017. An object-based approach for two-level gully feature mapping using high-resolution DEM and imagery: a case study on hilly loess plateau region, China. *Chinese Geographical Science*, 27(3): 415–430. doi: 10.1007/s11769-017-0874-x

Liu X Y, 2008. Airborne LiDAR for DEM generation: some critical issues. *Progress in Physical Geography*, 32(1): 31–49. doi: 10.1177/0309133308089496

MacMillan R A, Pettapiece W W, Nolan S C et al., 2000. A generic procedure for automatically segmenting landforms into landform elements using DEMs, heuristic rules and fuzzy logic. *Fuzzy Set and System*, 113(1): 81–109. doi: 10.1016/S0165-0114(99)00014-7

MacMillan R A, Shary P A, 2009. Chapter 9 Landforms and landform elements in geomorphometry. *Developments in Soil Science*, 33: 227–254. doi: 10.1016/S0166-2481(08)00009-3

Murphy P N, Ogilvie J, Meng F R et al., 2008. Stream network modelling using lidar and photogrammetric digital elevation models: a comparison and field verification. *Hydrological Processes: An International Journal*, 22(12): 1747–1754. doi: 10.1002/hyp.6770

Pirotti F, Tarolli P, 2010. Suitability of LiDAR point density and derived landform curvature maps for channel network extraction. *Hydrological Processes*, 24(9): 1187–1197. doi: 10.1002/hyp.7582

Qian Yeqing, Xiong Liyang, Li Jilong et al., 2016. Landform planation index extracted from DEMs: a case study in ordos platform of China. *Chinese Geographical Science*, 26(3): 314–324. doi: 10.1007/s11769-016-0811-4

Romstad B, Etzelmüller B, 2012. Mean-curvature watersheds: a simple method for segmentation of a digital elevation model into terrain units. *Geomorphology*, 139−140: 293–302. doi: 10.1016/j.geomorph.2011.10.031

Rossi C, Gonzalez F R, Fritz T et al., 2012. TanDEM-X calibrated Raw DEM generation. *ISPRS Journal of Photogrammetry and Remote Sensing*, 73: 12–20. doi: 10.1016/j.isprsjprs.2012.05.014

Schmidt J, Hewitt A, 2004. Fuzzy land element classification from DTMs based on geometry and terrain position. *Geoderma*, 121: 243–256. doi: 10.1016/j.geoderma.2003.10.008van

Schmidt J, Andrew R, 2005. Multi-scale landform characterization. *Area*, 37(3): 341–350. doi: 10.1111/j.1475-4762.2005.00638.x

Szypuła B, 2019. Quality assessment of DEM derived from topographic maps for geomorphometric purposes. *Open Geosciences*, 11(1): 843–865. doi: 10.1515/geo-2019-0066

Tao Yang, Tang Guoan, Strobl Josef, 2012. Spatial structure characteristics detecting of landform based on improved 3D Lacunarity model. *Chinese Geographical Science*, 22(1): 88–96. doi: 10.1007/s11769-012-0516-2

Tarolli P, 2014. High-resolution topography for understanding Earth surface processes: opportunities and challenges. *Geomorphology*, 216: 295–312. doi: 10.1016/j.geomorph.2014.03.008

Tarolli P, Sofia G, 2016. Human topographic signatures and derived geomorphic processes across landscapes. *Geomorphology*, 255: 140–161. doi: 10.1016/j.geomorph.2015.12.007

Whiteside T G, Boggs G S, Maier S W, 2011. Comparing object-based and pixel-based classifications for mapping savannas. *International Journal of Applied Earth Observation and Geoinformation*, 13(6): 884–893. doi: 10.1016/j.jag.2011.06.008

Wood J D, 1996. *The Geomorphologic Characterization of Digital Elevation Models*. Leicester: University of Leicester.

Yang J, Jin S H, Xiao X M et al., 2019. Local climate zone ventilation and urban land surface temperatures: towards a performance-based and wind-sensitive planning proposal in megacities. *Sustainable Cities and Society*, 47: 101487. doi: 10.1016/j.scs.2019.101487

Yang J, Luo X, Jin C et al., 2020. Spatiotemporal patterns of vegetation phenology along the urban-rural gradient in Coastal Dalian, China. *Urban Forestry & Urban Greening*, 54: 126784. doi: 10.1016/J.UFUG.2020.126784

Zhou X R, Li W W, Arundel S T, 2019. A spatio-contextual probabilistic model for extracting linear features in hilly terrains from high-resolution DEM data. *International Journal of Geographical Information Science*, 33(4): 666–686. doi: 10.1080/13658816.2018.1554814

Zhu Hongchun, Tang Guoan, Qian Kejian et al., 2014. Extraction and analysis of gully head of Loess Plateau in China based on digital elevation model. *Chinese Geographical Science*, 24(3): 328–338. doi: 10.1007/s11769-014-0663-8

Zhu L J, Zhu A X, Qin C Z et al., 2018. Automatic approach to deriving fuzzy slope positions. *Geomorphology*, 304: 173–183. doi: 10.1016/j.geomorph.2017.12.024

Zhu Y, Liu X J, Zhao J et al., 2019. Effect of DEM interpolation neighbourhood on terrain factors. *ISPRS International Journal of Geo-Information*, 8(1): 30. doi: 10.3390/ijgi8010030